Correlated ion stopping in a dense classical plasma

Claude Deutsch and Patrice Fromy
Laboratoire de Physique des Gaz et Plasmas, Associé au CNRS, Bâtiment 212, Université Paris XI, 91405 Orsay, France
(Received 20 July 1994)

The correlated ion stopping within N-clusters of ion debris, resulting from a swift fragmentation of a weakly ionized cluster impacting a dense and fully ionized classical plasma, is considered in the high velocity limit. Elaborating upon dicluster polarized stopping with a Fried-Conte plasma dielectric function, N-cluster stopping is taken as a linear superposition of every available dicluster pair. The main focus is on the enhanced correlation stopping and its dependence on N, N-cluster arrangement, as well as target plasma coupling. The main trends are qualitatively reminiscent of N-cluster stopping in a fully degenerate electron fluid. The basic length is the target electron screening length (Debye).

PACS number(s): 52.40.Mj, 34.50.Bw, 52.65.−y, 52.58.−c

I. INTRODUCTION

The linear acceleration of ionized clusters structures at energies of the order of a few tens of keV/amu is becoming presently a rather routine operation [1–5]. Among the many available cluster configurations, it is worthwhile to mention the fullerene, the carbonlike, and also the metallic ones such as Au_n^{q+} produced at high energy on tandem Van de Graaff accelerators.

It should be recalled that low-velocity acceleration is already well documented [6]. It offers many practical applications such as metal alloying, surface treatment, and preparation. Here we intend to focus on the interaction of more energetic particles with energy per nucleon $\gtrsim$ a few keV/amu. Then their interaction with cold or hot matter may be considered mostly as a stopping process through Coulomb interaction with target electrons. It is now quite a well accepted view that energetic clusters fragment very rapidly, on a femtosecond time scale [7], which yields a resulting Coulombic N cluster of ion debris flowing within a few a.u. of relative distance. The resulting correlated stopping in a dense and cold target has already been studied with a dielectric formulation for the electron fluid responsible for the projectile energy loss. Initially, investigations were mostly confined to dicluster stopping [8]. More recently, they have also been extended to arbitrarily large N clusters [9–15]. Then the conspicuous fact is the strong departure from single-ion energy loss through a simultaneous flow of closely connected pointlike ion charges. All the above-mentioned works are exclusively dedicated to cold matter stopping with a fully degenerate electron jellium at $T=0$. However, very recently, systematic attention has also been paid to dicluster stopping and the vicinage effect in a hot and dense classical electron fluid with a Maxwellian velocity distribution [16,17]. The main goal of the present work is to investigate N-cluster ions interacting with such a classical electron stopping medium by using a linear superposition of every available dicluster. Such a procedure has recently been the object of much attention at $T=0$ [13–15].

The basic physical situation we intend to model is the compression of thermonuclear and spherical pellets through intense cluster ion beams [9,13,14,18–20]. A huge hammerlike source of efficient shock waves has thus already been identified [13,19], which arises directly from the enhanced correlation stopping (ECS) alluded to previously. Those rather encouraging results are by now essentially documents for a $T=0$ target. So their potential extension to an arbitrarily hot plasma target is of a crucial significance in asserting the feasibility of particle-driven inertial confinement fusion through cluster ion beams. Such a statement stems from the obvious observation that the enormous compression expected through cluster beams will very rapidly heat cold target matter into a dense and hot ionized fluid. Here we restrict ourselves to a non-degenerate electron stopping medium, which is of relevance also for further applications in magnetically confined thermonuclear fusion [16,17].

This work is also motivated by an urgent request from several experimental groups [1–5] exploring the various aspects of cluster ion-dense matter interaction: acceleration, fragmentation, correlated stopping of resulting ion debris, etc. A reasonable predictive scheme based on a clear theoretical framework then may be extremely helpful in relating the observable parameters to theory. We think that it is of primary significance to investigate the dependence of the stopping of correlated ion debris on the initial projectile velocity, interdebris distances, the topology, and the target density.

In this regard, it appears very instructive to model the target by a dense and homogeneous electron plasma. It should also be appreciated that a systematic study of N-body correlations during cluster stopping has begun only very recently and has been restricted to the cold jellium limit ($T=0$).

In a broader perspective, it might also be stimulating to think of a possible connection between the stopping of a collection of correlated point charges with the interaction of a non-point-like and extended object interacting through the Coulomb law with a dense and fully ionized target. Such an analogy is likely to bring some insight into the crucial issues of high energy collisions involving the so-called elementary particles, which have a complex

structure (quarks plus gluons) and also the nuclei based on protons and neutrons.

Recently, we have also investigated dicluster ion energy loss in a partially degenerate electron fluid [21]. The corresponding N-cluster stopping is currently under investigation.

Dicluster stopping in a classical electron plasma according to the recent treatment by d'Avanzo, Lantano, and Bortignon [16,17], is briefly outlined in Sec. II as a preliminary step toward explaining N-cluster stopping as a linear superposition of dicluster contributions (Sec. III). The enhanced correlation stopping is then thoroughly documented (Sec. IV). Its specific dependence on N topological ion debris configurations (Sec. V), velocity, (Sec. VI) and target electron coupling is thus emphasized. The cubic box arrangement with eight unit charges often appears as a convenient working example. The specific ease afforded by N chains of identical point charges regularly spaced is also given due attention in Sec. VII. Final remarks are offered in Sec. VIII.

II. DICLUSTER STOPPING IN A CLASSICAL PLASMA

Here we briefly review a basic formulation for dicluster stopping in a dense and hot classical plasma [16,17] which parallels closely a similar derivation for a $T=0$ electron jellium [8]. The correlation contribution to stopping is conveniently highlighted by taking the ion pair in a cylindrical geometry (Fig. 1), defined by the common and overall drift velocity $\mathbf{V}$ and interparticle distance $\mathbf{R}$.

In this work, we neglect any velocity mismatch between the two charges Z_1 and Z_2. The corresponding straggling correction will be treated elsewhere. Preliminary considerations [22] show that if one writes the stopping power as $S=-\Delta E/\Delta x$, the magnitude of the mean energy loss per unit pathlength, one can define Ω^2 as the square of the standard deviation of the energy loss distribution per unit path length, i.e.,

$$\Omega^2=\frac{[\langle(\Delta E)^2\rangle-\langle\Delta E\rangle^2]}{\Delta x} .$$

It turns out that for a plasma target with $k_BT\gg E_F$ (the Fermi energy), one has, within a good approximation, $\Omega^2\sim 2k_BTS$. So computing the stopping power yields a reasonable estimate for the straggling. Moreover, in light of an experimental program developed on the Orsay tandem linear accelerator, we think it is useful to restrict our investigation to classical plasma targets of fully ionized deuterium at a rather moderate temperature T approximately equal to a few eV, where the corresponding free electron density ranges from 2×10^{17} up to 10^{20} cm^{-3}. At such modest temperatures, the straggling may thus be neglected in a first approximation.

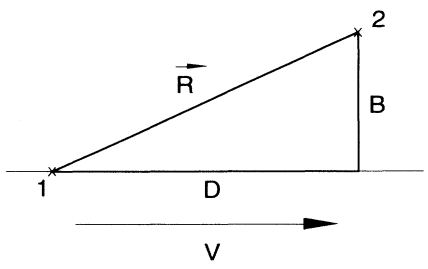

FIG. 1. Cylindrical coordinates along projectile velocity $\mathbf{V}$ for dicluster stopping with intercharges distance $\mathbf{R}$. B and D denote $\mathbf{R}$ projections perpendicular and parallel, respectively, to $\mathbf{V}$.

The dicluster stopping calculation starts with the electrostatic potential expressed in a reference system where the two ions are at rest [8,16,17] and the leading ion is located at the origin. It reads as (see Fig. 1)

$$\phi_1(\mathbf{r})=\frac{1}{(2\pi)^3}\int d^3\mathbf{k}\frac{e^{i\mathbf{k}\cdot\mathbf{r}}}{k^2\varepsilon(k,\mathbf{k}\cdot\mathbf{V})}(Z_1+Z_2e^{-i\mathbf{k}\cdot\mathbf{R}}) , \quad (1)$$

where

$$\varepsilon(k,\omega)=1+w\left[\frac{\omega}{k}\right]\frac{1}{k^2}, \quad w(\xi)\equiv X(\xi)+iY(\xi) \quad (2)$$

denotes the longitudinal dielectric function for a Maxwellian and classical electron plasma [23].

The physics of the problem relies heavily on an adequate scaling of the dynamic variables, so it is very useful to work in the so-called plasma units with dimensionless variables [16,17]

$$r\to\frac{r}{\lambda_D}, \quad t\to\omega_p t, \quad \mathbf{V}\to\frac{\mathbf{V}}{\mathbf{V}_{\rm th}}, \quad \phi\to\frac{e}{k_BT}\phi , \quad (3)$$

where

$$\lambda_D=\left[\frac{k_BT}{4\pi n_e e^2}\right]^{1/2}=7.43\times10^2\frac{[T\ (\mathrm{eV})]^{1/2}}{[n_e\ (\mathrm{cm}^{-3})]^{1/2}}$$

is the Debye electron screening length,

$$N_D=n_e\lambda_D^3=\frac{3}{4\pi}\times1.72\times10^9\frac{[T\ (\mathrm{eV})]^{1/3}}{[n_e\ (\mathrm{cm}^{-3})]^{1/2}}$$

is the number of electrons within a Debye sphere,

$$\omega_p=5.69\times10^4[n_e\ (\mathrm{cm}^{-3})]^{1/2}\ \frac{\mathrm{rad}}{\mathrm{sec}}$$

is the electron plasma frequency, and $V_{\rm th}=\sqrt{k_BT/m_e}$ is the thermal electron velocity. From the above parameters, it is also convenient to introduce the dimensionless combination

$$\Lambda=\frac{e^2}{k_BT\lambda_D}=2.05\times10^{-10}\frac{[n_e\ (\mathrm{cm}^{-3})]^{1/2}}{[T\ (\mathrm{eV})]^{3/2}}$$

measuring the strength of Coulomb coupling. Within the present (T,n_e) values of interest, one typically has $0.03\le\Lambda\le0.23$. The weakly coupled plasma target is thus characterized by the Fried-Conte expression [23]

$$w(\xi)\equiv X(\xi)+iY(\xi)$$
$$=\frac{1}{\sqrt{2\pi}}\lim_{\nu\to0}+\int_{-\infty}^{\infty}\frac{dx\,xe^{-x^2/2}}{x-\xi-i\nu} ,$$
$$=i\left[\frac{\pi}{2}\right]^{1/2}\xi e^{-\xi^2/2}+1-\xi e^{-\xi^2/2}\int_0^{\xi}dy\,e^{y^2/2} , \quad (2')$$

which simplifies when $\xi \ll 1$ to the form

$$w(\xi)=i\left[\frac{\pi}{2}\right]^{1/2}\xi e^{-\xi^2/2}+1-\xi^2+\frac{\xi^4}{3}+\cdots+(-)^{n+1}\frac{\xi^{2n+2}}{(2n+1)!!}+\cdots, \quad (2'')$$

According to Fig. 1, the dicluster stopping is defined by

$$-\frac{dE}{dx}=Z_1N_D\frac{\partial\phi_{\rm ind}}{\partial\mathbf{r}}\bigg|_{\mathbf{r}=\mathbf{r}_1(t)}+Z_2N_D\frac{\partial\phi_{\rm ind}}{\partial\mathbf{r}}\bigg|_{\mathbf{r}=\mathbf{r}_2(t)}, \quad (4)$$

where $\mathbf{r}_1(t)=\mathbf{V}t$ and $\mathbf{r}_2(t)=\mathbf{V}t+R$, respectively. $\phi_{\rm ind}$ denotes the electrostatic potential of one unit charge acting on the other. So, from expression (1), one derives [8,16,17]

$$-\frac{dE}{dx}=\frac{N_D}{(2\pi)^3}\int d^3\mathbf{k}\frac{i\mathbf{k}\cdot\mathbf{V}}{V}\frac{1}{k^2}\left[\frac{1}{\varepsilon(\mathbf{k},\mathbf{k}\cdot\mathbf{V})}-1\right]\times[Z_1^2+Z_2^2+2Z_1Z_2\cos(\mathbf{k}\cdot\mathbf{R})]. \quad (5)$$

Setting $Z_1=Z_2=Z$ and making use of Eq. (2) one gets

$$-\frac{dE}{dx}=\frac{Z^2N_D}{\pi^2}\int_0^{k_{\max}}dk\,k^3\int_0^1\frac{d\mu Y(\mu V)}{[k^2+X(\mu V)]^2+Y^2(\mu V)}[1+\cos(k\mu D)J_0(k\sqrt{1-\mu^2}B)]$$
$$\equiv 2Z^2S(1)+2Z^2S_V(B,D)=\mathcal{S}_{\rm point}+\mathcal{S}_{\rm corr} \quad (6)$$

in terms of the ordinary Bessel function $J_0(x)$ and $k_{\max}=4\pi(V^2+2)N_D/Z$.

Also, we have split the correlation $\mathcal{S}_{\rm corr}$ contribution to stopping from the uncorrelated pointlike $\mathcal{S}_{\rm point}$ contribution. B and D are the transverse and longitudinal projections of $\mathbf{R}$ on $\mathbf{V}$, respectively (Fig. 1). At this juncture, it is worthwhile to notice that the presently considered frozen geometry (Fig. 1) is well justified because we are restricted to a high velocity range for the projectile. For instance, if one considers a dicluster with a 10 keV/amu kinetic energy and if we admit that the Coulomb repulsion potential within ion pairs contributes to a velocity transverse to $\mathbf{V}$, one has approximately $V_\perp/V \cong 0.79ZA^{-1/2}$, where A is the cluster ion atomic mass. So the present polarized approximation appears well justified for heavy ion fragments with $A \gg 1$ and not for hydrogen fragments [5].

III. *N*-CLUSTER STOPPING

Now we consider the simultaneous stopping of N ion debris flowing with the same projectile velocity V in close proximity to each other, i.e., within a few a.u. of relative distance. A first and obvious extension of the above, polarized two-body treatment is to superimpose the $N(N-1)/2$ dicluster energy losses available in a Coulomb N cluster.

Such a simple generalization has already produced a huge variety of charge configurations leading to the ECS, in cold target stopping [8–15,24] provided $N>2$. Rewriting the second right-hand side of Eq. (6) for two distinct charges, one retrieves

$$-\frac{dE}{dx}=(Z_1^2+Z_2^2)S(1)+2Z_1Z_2S_v(B,D) \quad (7)$$

and the corresponding N-cluster expression in then obtained as

$$-\frac{dE}{dx}=\sum_{i=1}^{N}Z_i^2S(1)+2\sum_{1\le i<j\le N}Z_iZ_jS_v(B_{ij},D_{ij})$$
$$\equiv\mathcal{S}_{\rm point}+\mathcal{S}_{\rm corr}=\mathcal{S}_{\rm stop}. \quad (8)$$

As shown by previous studies of the ECS in a degenerate jellium target [13], it will prove useful to quantify the expected ECS through a few obvious ratios. The first one reads as

$$\mathcal{R}_1=\frac{\mathcal{S}_{\rm corr}}{\mathcal{S}_{\rm stop}}\le 1-\frac{\sum_{i=1}^{N}Z_i^2}{\left[\sum_i Z_i\right]^2}, \quad (9)$$

in terms of the total stopping $\mathcal{S}_{\rm stop}$. An obviously related quantity of great interest is

$$\mathcal{R}_2=\frac{\mathcal{S}_{\rm corr}}{\mathcal{S}_{\rm point}}=\frac{\mathcal{R}_1}{1-\mathcal{R}_1}\le\frac{\left[\sum_i Z_i\right]^2}{\sum_i Z_i^2}-1, \quad (10)$$

denoting the ratio of correlated to uncorrelated stopping. Also instructive is the average correlation contribution

$$\bar{\mathcal{S}}_{\rm corr}=2\sum_{1\le i\le j\le N}\frac{\mathcal{S}_{\rm corr}(i,j)}{N(N-1)}. \quad (11)$$

The ratios (9)–(11) are independent of target coupling. They also apply to a $T=0$ jellium target [13] and to a partially degenerate electron fluid as well. They produce *a priori* guidelines of great interest for the ECS numerical estimation.

For instance, symmetrical charge configurations with $Z_1=Z_2=\cdots=Z_N\equiv Z$ fulfill $\mathcal{R}_1\le 1-N^{-1}$ and $\mathcal{R}_2\le N-1$. In this case, one has $0.666\le\sup(\mathcal{R}_1)\le 1$ with $3\le N\le\infty$. Selecting highly dissymmetric distributions with $Z_1=Z_2=\cdots=Z_{N-1}=1$ and $Z_N=N$, one witnesses $0.59\le\sup(\mathcal{R}_1)\le 0.75$ with $3\le N\le\infty$. As a consequence, one is led to identify symmetric configurations as those providing the highest correlated stopping.

Before detailing the numerical and physical content of expression (8), it should be mentioned that we have intentionally left aside the important discussion about its validity when arbitrarily large Z_i values are introduced in

it. Here we take the simple view that projectile charges are fixed during the stopping process and we push the present linear analysis to its limits in order to unravel the specific qualitative and semiquantitative features of correlated ion species in the high velocity range of present interest.

IV. ENHANCED CORRELATION STOPPING

A. Dicluster

Before embarking into an extensive study of N-cluster stopping, it is highly instructive to investigate through Eqs. (6) and (7) the dicluster ECS, in terms of overall velocity V and relative distance $\mathbf{R}$. Figures 2(a) and 2(b) feature two target plasmas at $T=2$ eV. The first one is with $n_e=2\times10^{17}$ cm^{-3}. The ratio $\mathcal{R}_2$ [Eq. (10)] is then depicted in terms of B/λ_D and $V/V_{\rm th}$ at a fixed interchange distance $R=\lambda_D$. Already there is an ECS of the order of 30% on most of the parameter's range. ECS increases steadily with V up to a nearly constant plateau value. Also, for small $V/V_{\rm th}$ ($\lesssim 5$) one observes a larger stopping for an oblique dicluster than for a parallel one, with respect to $\mathbf{V}$. Finally, the correlation stopping also seems to increase with plasma coupling Λ. It is useful to

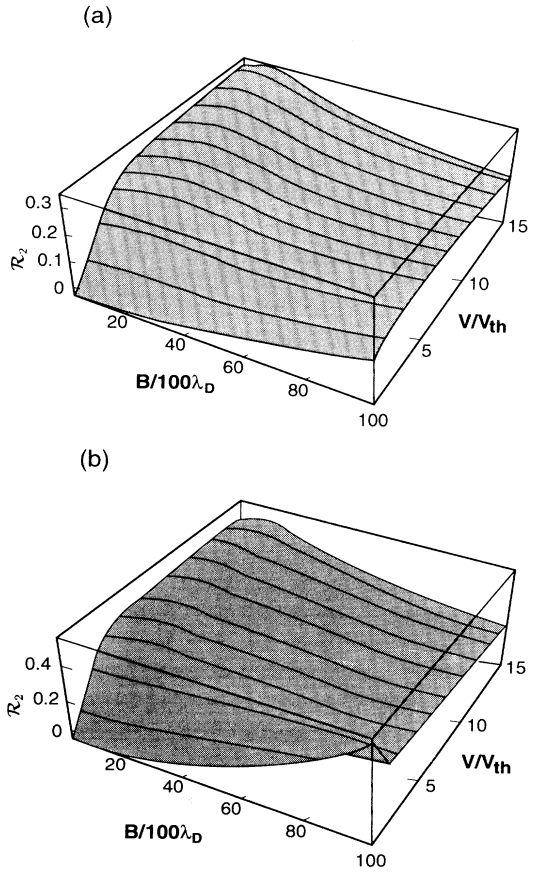

FIG. 2. (a) Ratio $\mathcal{R}_2$ [Eq. (10)] for a dicluster with $Z_1=Z_2=Z$ and $R=\lambda_D$ in terms of $B/100$ in λ_D and V in $V_{\rm th}$. $T=2$ eV and $n_e=2\times10^{17}$ cm^{-3}. (b) Same as (a), but with $T=2$ eV and $n_e=10^{20}$ cm^{-3}.

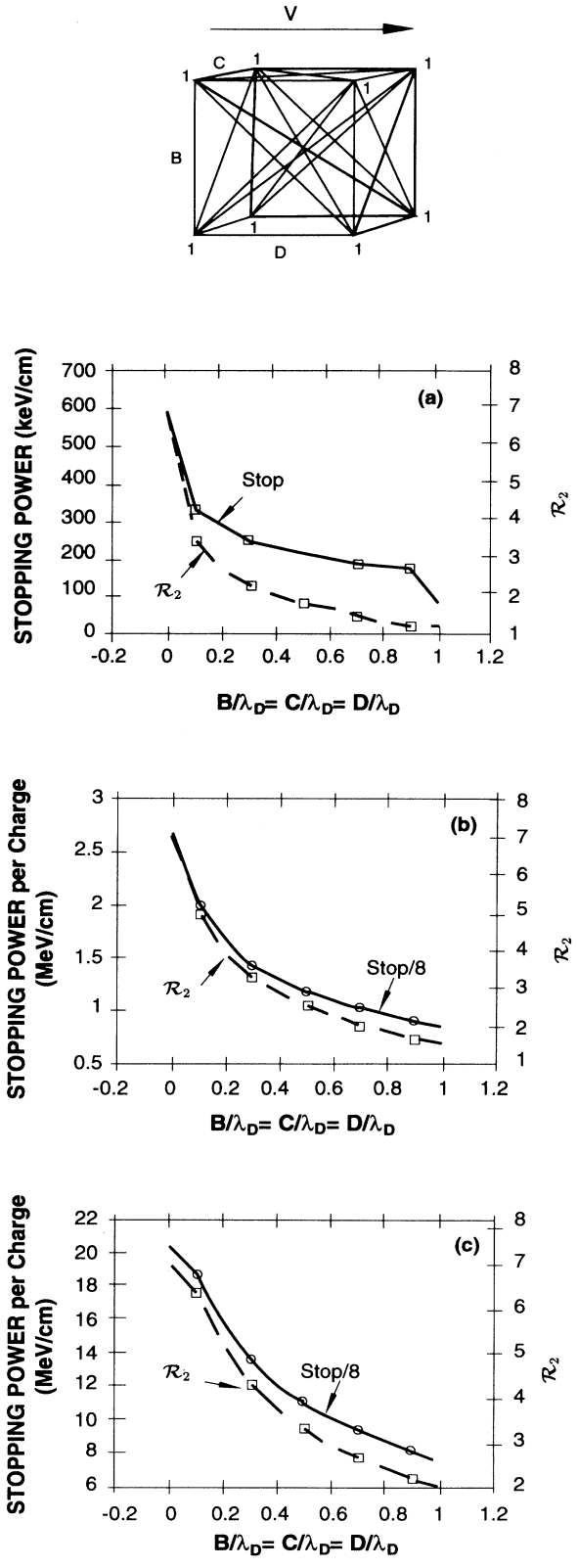

FIG. 3. Stopping $\mathcal{S}_{\rm stop}$ of eight unit charges and ratio $\mathcal{R}_2$ [Eq. (10)] arranged on a cubic box with sides ranging from 0 to λ_D. $V=3V_{\rm th}$ and $T=2$ eV. $D\|V$. (a) 2×10^{17} cm^{-3}, (b) $n_e=10^{19}$ cm^{-3}, and (c) $n_e=10^{20}$ cm^{-3}.

recall that a plasma with $T=2$ eV and $n_e=2\times10^{17}$ cm^{-3} has $V_{\rm th}=0.25$ a.u. and $\lambda_D=444$ a.u.

B. Cubic box

From the above, it is clear that a mere two-body vicinage effect brings in a substantial ECS. So now we implement the N-cluster stopping through Eq. (8). In order to emulate a typical arrangement of closely packed ion debris, we found it very instructive to look at a cubic display of eight unit pointlike charges at vertices, as shown on Fig. 3.

The given cubic box has a side $B=C=D$ running from 0 to λ_D. The projectile velocity is $V=3V_{\rm th}$. As before, $\mathbf{D}\|\mathbf{V}$, while B and C denote the two transverse dimensions.

At complete coagulation ($B=C=D=0$) the ECS fulfills the upper bounds (9) and (10) for a symmetric charge distribution with $\mathcal{R}_2=7$ at any target density. When the intercharge distances increase, total stopping and ECS decay as well. Nonetheless, even at the largest size ($B=C=D=\lambda_D$), the ECS remains at work with $\mathcal{R}_2\geq1$. It should be kept in mind that for the given plasma targets, the ion debris relative distances are large on an atomic scale (of the order of several tens of a.u.). The strongest stopping variations obtains at the smallest density ($n_e=2\times10^{17}$ cm^{-3}), where λ_D is largest.

Even more impressive ECSs are obtained for the restricted range $0\leq B=C=D\leq0.1\lambda_D$ (closer to the coagulation limit) (see Fig. 4) with $\mathcal{R}_2\geq3.5$ Figures 3 and 4 demonstrate clearly the dominant role played by the plasma screening λ_D in asserting the ECS performances of dense plasma stopping. It is also highly instructive to expand the cubic eight clusters far beyond λ_D, as shown in Fig. 5, at largest Λ coupling. As excepted the stopping charge decays to the isolated charge value while $\mathcal{R}_2$ rapidly oscillates around zero, with $\mathcal{R}_2>0$, when $B=C=D\leq4\lambda_D$. However, the given decay is not abrupt and the ECS remains present at nearest-neighbor distances larger than λ_D.

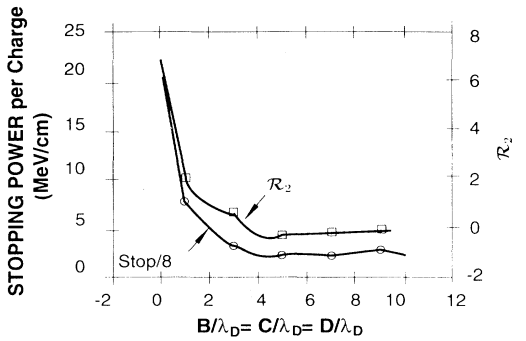

FIG. 5. Same as Fig. 3, but with sides from 0 to $10\lambda_D$. $n_e=10^{20}$ cm^{-3}.

C. Shape dependence

In order to assert the ECS universality beyond overall dilation of a regular and symmetric charge distribution, we now pay attention to partial dilation. Then, in Fig. 6, we first keep B and C constant with $0\leq D\leq\lambda_D$ and then consider the opposite case with D fixed. Variations are

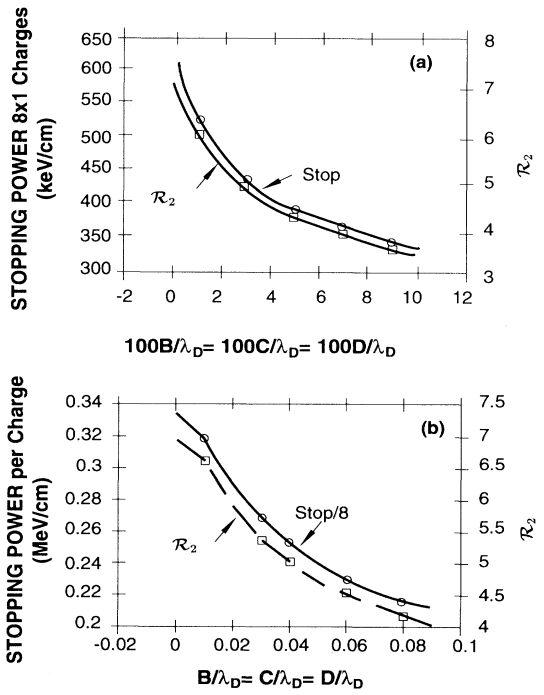

FIG. 4. Same as Fig. 3, but with sides ranging from 0 to $0.1\lambda_D$. (a) $n_e=2\times10^{17}$ cm^{-3} and (b) $n_e=10^{18}$ cm^{-3}.

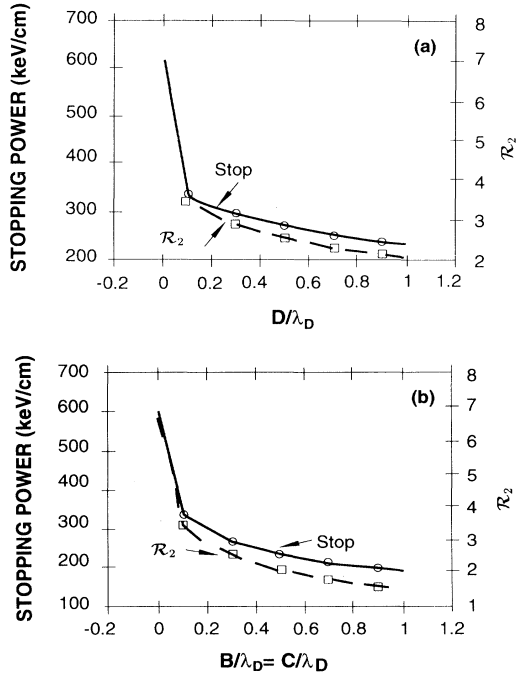

FIG. 6. Same as Fig. 3. $T=2$ eV, $n_e=2\times10^{17}$ cm^{-3}, and $V=3V_{\rm th}$. (a) $B=C=0.1\lambda_D$, D ranges between 0 and λ_D; (b) $D=0.1\lambda_D$, $B=C$ ranges between 0 and λ_D.

pretty similar in both cases. However, in Fig. 6(a), one has $\mathcal{R}_2 > 2$, while it decreases below 2 for a transverse dilation [Fig. 6(b)].

Closely related behaviors are reported in Fig. 7 at the highest $n_e = 10^{20}$ cm^{-3}. Again, one notices that $\mathcal{R}_2 \geq 3.5$ for longitudinal dilation, while it stays around 3 for $B = C = \lambda_D$ in the transverse case [Fig. 7(b)]. Figures 7(a) and 7(b) may also be fruitfully contrasted to their symmetric counterpart [Fig. 3(c)].

V. TOPOLOGICAL DEPENDENCE

At this juncture there is an obvious need for emphasizing the relative stopping capabilities of several topologically distinct configurations of eight unit charges, interacting at same velocity $V = 3V_{\rm th}$ with the same electron plasma target and with identical nearest-neighbor distances. So we now contrast the cubic box with regular arrays of pointlike charges propagating either parallel or transverse to the overall velocity **V**. Figure 8 display four target electron densities available on linear plasma column and Z-pinch devices installed on ion accelerator beam lines. A first overall and striking observation is afforded by the rather scale invariant increase with N stopping per charge, although that value differs by nearly an order of magnitude. Also, the order of the relative stopping efficiencies remains unchanged as n increases. Despite the fact that the three topologies considered share the same connectivity, the cubic box is the best performer because its charge-charge distances are more compactly distributed than in linear arrays. In the last two, the transverse N chain exhibits the second largest stopping.

Reducing the nearest-neighbor distance by a factor of 10 brings the stopping closer to its coagulation limit, where the topology does not matter much any more. Then the maximum and overall extension of the given N cluster is at best $0.1\lambda_D$. Figures 9(a) and 9(b) depicts such an option at $n_e = 10^{19}$ and 10^{20} cm^{-3}, respectively.

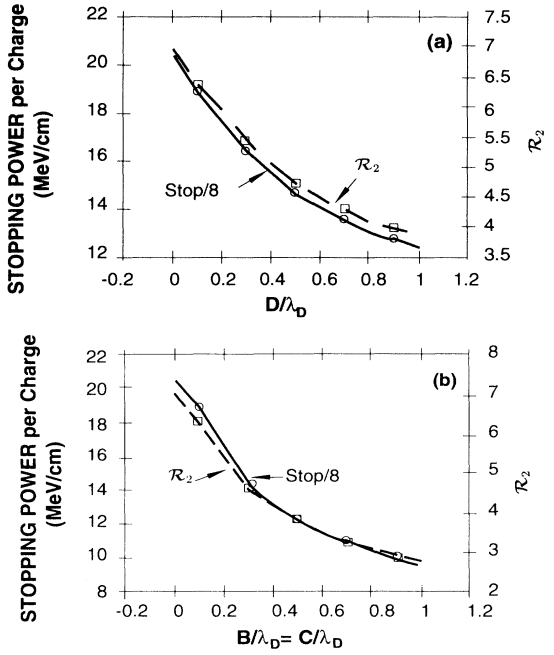

FIG. 7. Same as Fig. 6, but $n_e = 10^{20}$ cm^{-3}.

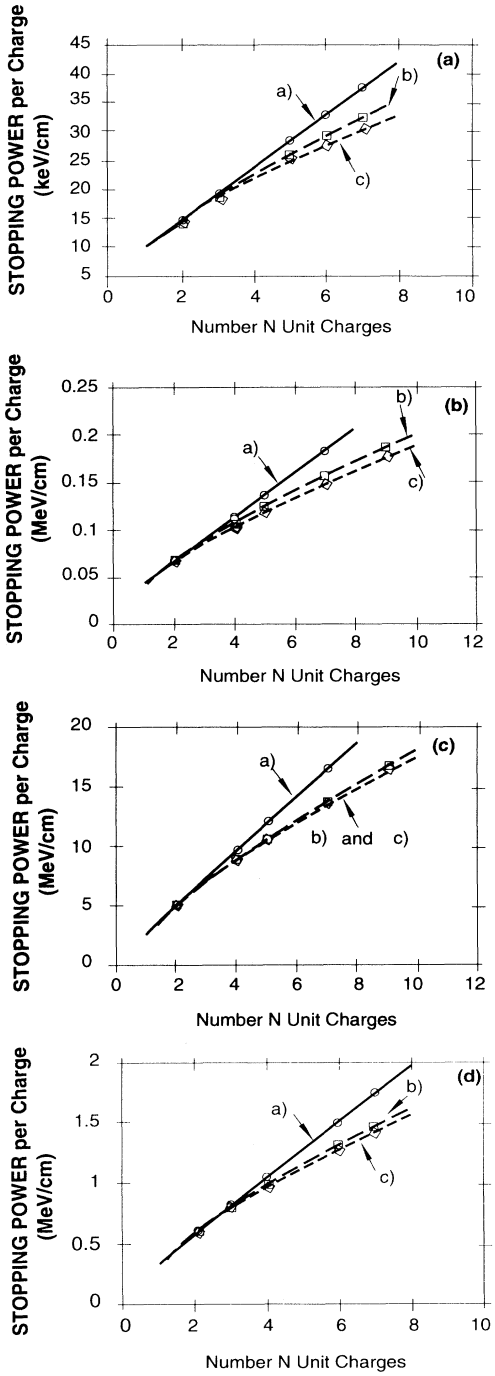

FIG. 8. Stopping of N clusters in terms of N with $B = C = D = 0.1\lambda_D$ and $V = 3V_{\rm th}$. $T = 2$ eV. $D \| V$. *a*, cubic box; *b*, transverse N chain; *c*, longitudinal N chain. (a) $n_e = 2 \times 10^{17}$ cm^{-3}, (b) $n_e = 10^{18}$ cm^{-3}, (c) $n_e = 10^{19}$ cm^{-3}, and (d) $n_e = 10^{20}$ cm^{-3}.

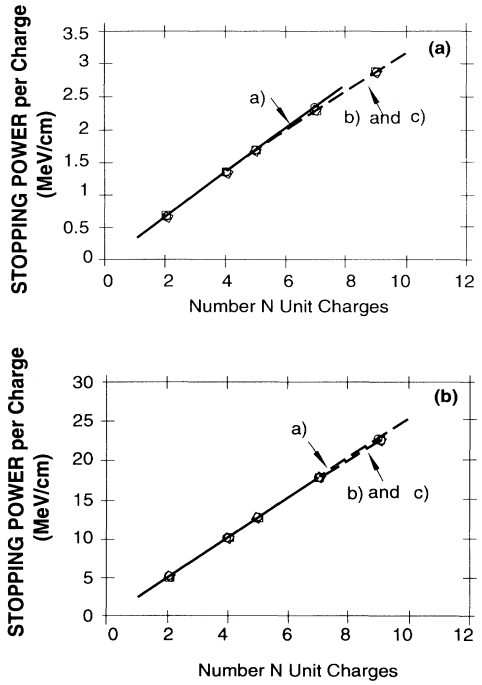

FIG. 9. Same as Fig. 8, but with $B=C=D=0.01\lambda_D$. (a) $n_e=10^{19}$ cm^{-3} and (b) $n_e=10^{20}$ cm^{-3}.

The different charge configuration experiences, practically the same stopping.

Again it proves rather illuminating to explore the opposite situation (Fig. 10) with a large size ($B=C=D=\lambda_D$). Now the behavior is at variance with previous ones, so the topology manifests itself globally. The overall N cluster now extends over several screening lengths. The order of relative stopping efficiency remains unchanged.

Curves b and c in Fig. 10 anticipate specific N-chain trends detailed below. Those results demonstrate once more that the ECS remains non-negligible at large particle interdistances.

Additional insight may also be obtained by looking at the average correlation contribution $\bar{\mathcal{S}}_{\rm corr}$ (Fig. 11). In Fig. 11 we have a box distribution. The quantities (9) and

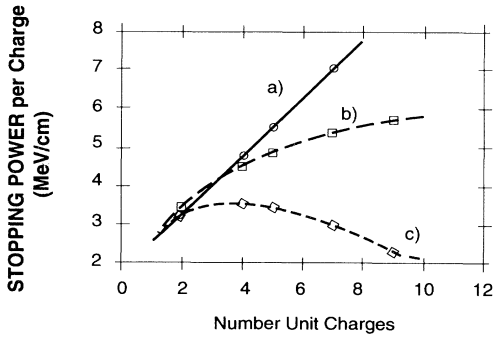

FIG. 10. Same as Fig. 8, but with $B=C=D=\lambda_D$. $n_e=10^{20}$ cm^{-3}.

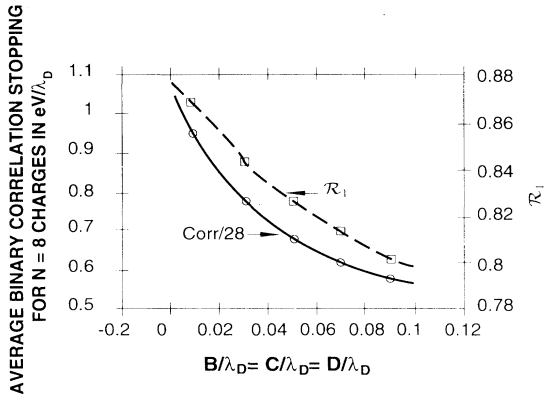

FIG. 11. Average binary correlation stopping $\bar{\mathcal{S}}_{\rm corr}$ [Eq. (11)] and correlation ratio $\mathcal{R}_1$ [Eq. (9)] in terms of side length for a cubical arrangement of eight unit charges. $V=3V_{\rm th}$. $T=2$ eV. Same parameters as in Fig. 8, but with $B=C=D=0.1\lambda_D$ and $n_e=10^{18}$ cm^{-3}. $D\|V$.

(11) featuring the ECS are given on the left and the right vertical axis, respectively. The huge correlation ratio $\mathcal{R}_1\geq 0.8$ pertains to a small cluster, close to coagulation. Nevertheless, the average correlation contribution to stopping $\bar{\mathcal{S}}_{\rm corr}$ still rapidly decays when size increases.

The cubic box and the two line arrays are compared in Fig. 12. The cubic arrangement features a nearly constant average correlated stopping in terms of the number of particles N. The linear arrays experience a monotone decay, in agreement with a much wider distribution of dicluster interdistances.

VI. VELOCITY DEPENDENCE

Up to now we have restricted the study to a fiducial velocity fixed at $V=3V_{\rm th}$. This convenient limitation does not invalidate the generality of our results, which are typical of a Bethe-like behavior with a V^{-2} prefactor in the

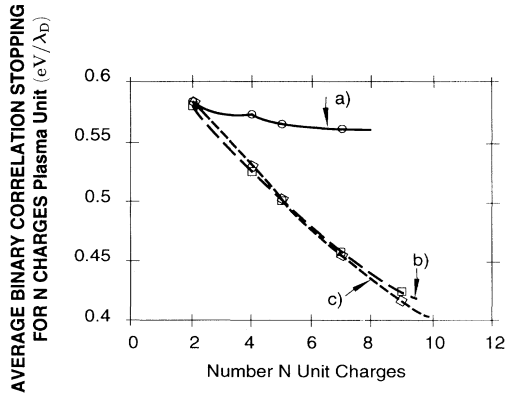

FIG. 12. Average binary correlation stopping [Eq. (11)] for N clusters in terms of N unit charges located on a cubic and linear arrays respectively transverse and parallel to $\mathbf{V}$. $V=3V_{\rm th}$, $T=2$ eV, and $n_e=10^{20}$ cm^{-3}. $D\|V$. a, cubic box; b, line $\perp V$; c line $\|V$.

stopping expression (7).

However, in the present context, where we stress out enhanced stopping, we think it relevant to prove the V dependence *per se* in a wide range. Figure 13 documents the corresponding expectation for $3 \leq V \leq 15$ in V_{th}. Figure 13(a) features first a cubic arrangement of eight unit charges with side $0.1\lambda_D$ stopped in an electron gas with $n_e = 2\times10^{17}$ cm^{-3}. We observe a Berthe-like stopping decay ($\sim V^{-2}$), while the correlation ratio $\mathcal{R}_2$ ranges between 3.5 and 0.5. Figure 13(b) extends the same interaction geometry to a denser target ($n_e = 10^{19}$ cm^{-3}). The stopping behavior seems to be very similar to the preceding one. However, now the ECS gets much higher with $\mathcal{R}_2 \geq 3.3$. A similar situation is afforded by Fig. 13(c) with a box side $\sim\lambda_D$ in a dense ($n_e = 10^{20}$ cm^{-3}) electron target.

Qualitatively, total stopping and correlation ratio

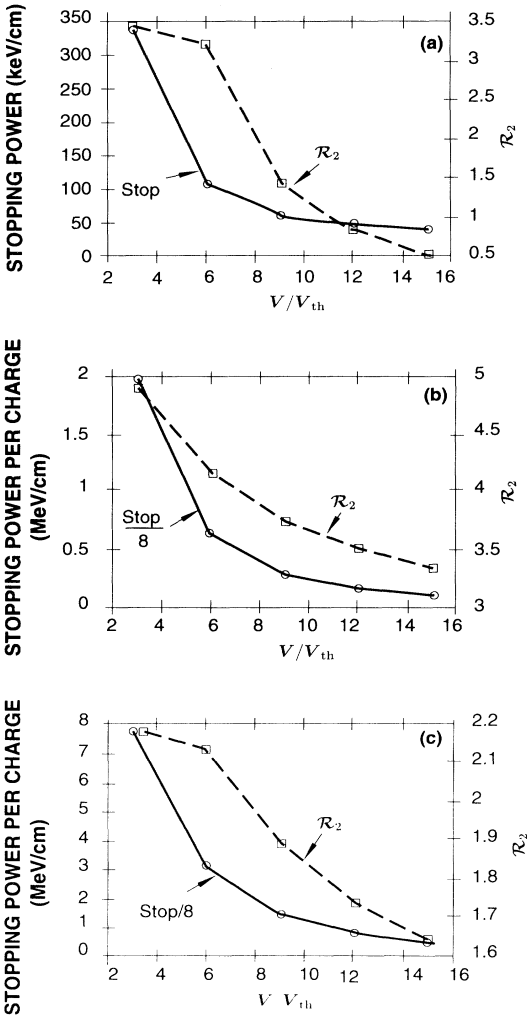

FIG. 13. Stopping power and correlation ratio $\mathcal{R}_2$ for eight unit charges at vertices of a cubic box in terms of projectile velocity V. $T=2$ eV. $D \| V$. (a) $B=C=D=0.01\lambda_D$ and $n_e=2\times10^{17}$ cm^{-3}, (b) $B=C=D=0.01\lambda_D$ and $n_e=10^{19}$ cm^{-3}, and (c) $B=C=D=\lambda_D$ and $n_e=10^{20}$ cm^{-3}.

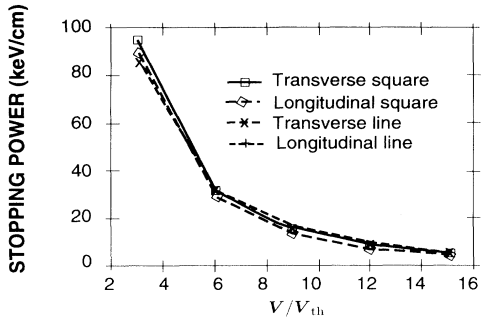

FIG. 14. Stopping of four clusters with various shapes and orientations relative to **V**. $B=D=0.1\lambda_D$. $T=2$ eV and $n_e=2\times10^{17}$ cm^{-3}.

displays rather close agreement. Again, we see that the large size of the ion cluster does not prevent it from experiencing an ECS with $\mathcal{R}_2 > 1.6$ at $V=15$. Moreover, we also found it instructive to test the V variations of four clusters, which included squares with sides $0.1\lambda_D$, respectively orthogonal and parallel to V, together with linear chains of regularly spaced unit charges, propagating either parallel or orthogonal to **V**.

The results shown in Fig. 14 are rather conclusive. In the given target ($n_e=2\times10^{17}$ cm^{-3}), there is practically no way for distinguishing one of the four clusters from the others.

VII. N CHAINS

The easiest fashion within the present approach to test the stopping N dependence is to investigate the behavior of N chains of unit charges regularly spaced and flowing either along **V** or transverse to it. We already detailed at length the corresponding study in the fully degenerate ($T=0$) case [24].

In Fig. 15 we see N chains, with $N \leq 20$, propagating parallel to **V**. They exhibit a steady stopping increase with N. The target plasma with $T=2$ eV and $n_e=10^{18}$ cm^{-3} is typical of what can be achieved in a stabilized Z-pinch discharge with a number $N_D=1.16$ of electrons in the Debye sphere. The nearest-neighbor distance is $D=0.1\lambda_D$.

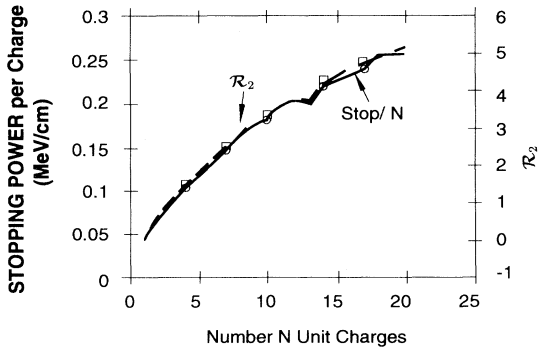

FIG. 15. Stopping N chains parallel to **V**. $V=3V_{\text{th}}$. $T=2$ eV and $n_e=10^{18}$ cm^{-3}. $D=0.1\lambda_D$.

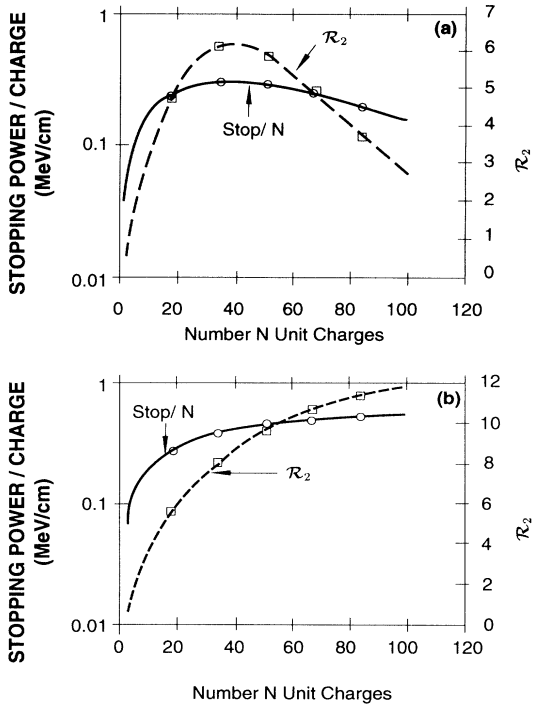

FIG. 16. Stopping N chains and correlation ratio $\mathcal{R}_2$ [Eq. (10)] with $N \leq 100$ and monomer length $0.1\lambda_D$. $V=3V_{\rm th}$. $T=2$ eV and $n_e=10^{18}$ cm^{-3}. (a) N chains $\|\mathbf{V}$ and (b) N chains $\perp\mathbf{V}$.

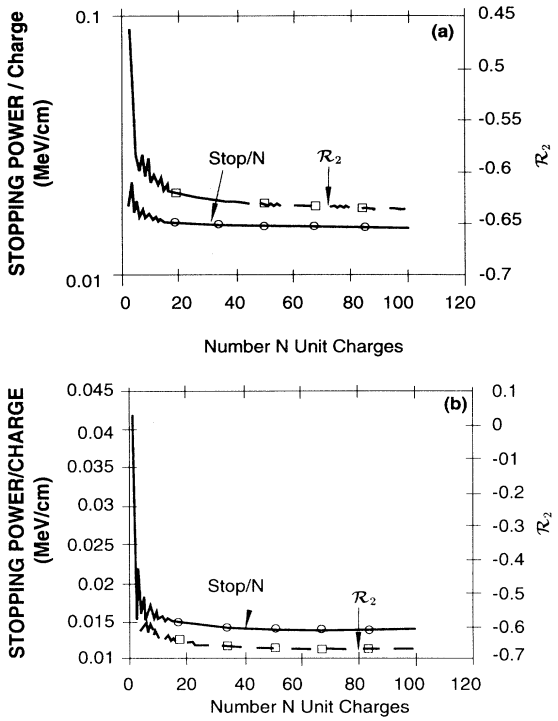

FIG. 18. Stopping N chains of unit charges of either sign and ratio $\mathcal{R}_2$ [Eq. (10)] with monomer length $0.1\lambda_D$, in terms of N. $V=3V_{\rm th}$. $T=2$ eV and $n_e=10^{18}$ cm^{-3}. (a) $D=0.1\lambda_D$, chains along $\mathbf{V}$; (b) $B=0.1\lambda_D$, chains transverse to $\mathbf{V}$.

In order to check the monotone increase for larger N values, we display in Fig. 16 similar results up to $N=100$ for both longitudinal and transverse N chains. Figure 16(a) makes it clear that the stopping per charge saturates around $N\sim 30-50$ and then starts decreasing. The ECS, through $\mathcal{R}_2$, follows and even accentuates that trend. Such behaviors replicate to a large extent the oscillating patterns for longitudinal N chains in a $T=0$ target [24].

On the other hand, transverse N chains also behave similarly to their $T=0$ counterparts [24]. The stopping per particle quickly rises up to a high plateau value, with an ever increasing ECS. As in the $T=0$ case, one may say that N-chain longitudinal transport is essentially monitored, as N increases, by fewer and fewer particles working out a path in the stopping medium. Most of the remaining particles are just surfing on the wake produced by a few forerunners. This behavior illustrates a very large but negative correlation stopping.

In contradistinction, in the transverse case, each particle has to develop for itself a path in a target in same state. Then, the N-chain effect manifests itself through a very large positive ECS.

As above, it also proves useful to pay attention to correlation stopping per number of available diclusters [Eq. (11)] within N chains (see Fig. 17) in terms of N. N is shown to decay smoothly. C_N^2 denotes $N(N-1)/2$. Finally, we think that it is also worthwhile to mention an obvious extension of the present study to globally neutral N chains built on alternate unit charges of either sign. The longitudinal one is given in Fig. 18(a). The corresponding stopping drops rapidly to a plateau value below the isolated charge value, which demonstrates a negative ECS. Here the transverse N chain behaves in pretty much the same fashion. In both cases, the smallest particle interdistance is $B=D=0.1\lambda_D$ and the chain orientation with respect to $\mathbf{V}$ produces quite a difference.

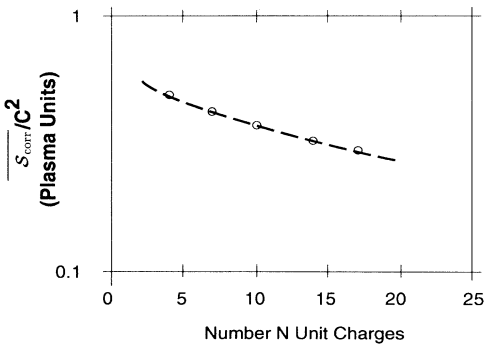

FIG. 17. Average binary correlation stopping [Eq. (11)] for N chains along $\mathbf{V}$ ($V=3V_{\rm th}$) in terms of N. $T=2$ eV and $n_e=10^{18}$ cm^{-3}.

VIII. CONCLUDING REMARKS

We made use of a complete random phase approximation for the linear response of a dense classical electron target in order to estimate the interaction with incoming

Coulomb N clusters of ion debris. The given stopping is taken in a high velocity formalism based on a linear super-position of every correlated dicluster contribution within N clusters. We restricted the study to equal distributions of unit charges in order to emphasize the basic features and properties of the enhanced correlation stopping such as ion debris topology and target plasma coupling.

The nearly ubiquitous ECS is thus expected to be of considerable and potential significance in providing new range-energy relationships useful in designing novel scenarios of interest for the cluster ion beam-dense matter interaction in particle-driven inertial confinement fusion. The presently considered model bears a direct relevance to the plasma phases of the compressed pellet containing the thermonuclear fuel.

As mentioned in the Introduction, our simple model of correlated ion stopping in a dense and fully ionized plasma should be able to provide preliminary and useful guidance to experimentalists aiming at measuring carefully the energy and orientation of ion debris fragmentated after a Coulomb explosion has taken place in the initial cluster projectile [1–5]. In this regard, it is also worthwhile to notice that ion debris of equal charges and the same velocity are likely to build up regular N-cluster structures as long as the target is taken in the one component plasma model [26]. Then the ion-ion Coulomb repulsion is compensated for by the target electron jellium. Thus one can expect a significant ECS on the projectile trajectory in target.

[1] P. Attal, S. Della-Negra, D. Gardès, J. D. Larson, Y. Le Beyec, R. Vienet-Lequé, and B. Waast, Nucl. Instrum. Methods A **238**, 293 (1993).
[2] S. Della-Negra, A. Brunelle, Y. Le Beyec, J. M. Curaudeau, J. P. Mouffron, B. Waast, P. Håkanson, B. V. R. Sundquist, and E. Parilis, Nucl. Instrum. Methods B **74**, 453 (1993).
[3] K. Boussofiane-Baudin, A. Brunelle, P. Chaurand, J. Depauw, S. Della-Negra, P. Håkanson and Y. Le Beyec, Int. J. Mass Spectrosc. Ion Processes **130**, 73 (1994).
[4] Ch. Schoppmann, P. Wohlfart, D. Brandl, M. Sauer, Ch. Tomaschko, H. Voit, K. Boussofiane, A. Brunelle, P. Chaurand, J. Depauw, S. Della-Negra, P. Håkanson, and Y. Le Beyec, Nucl. Instrum. Methods B **82**, 156 (1993).
[5] M. Farizon, N. V. De Castro Farcia, B. Farizon-Mazuy, and M. J. Gaillard, Phys. Rev. **45**, 179 (1992).
[6] Proceedings of a Conference on Polyatomic Ion Impact on Solids and Related Phenomena, Saint Malo, France, 1993 [Nucl. Instrum. Methods B **88**, 1 (1994)].
[7] D. Kella, M. Algranati, H. Feldman, O. Heher, H. Kovner, E. Malkin, E. Miklazky, R. Naaman, D. Zajfman, J. Zajfman, and Z. Vager, Nucl. Instrum. Methods A **329**, 440 (1993).
[8] G. Basbas and R. H. Ritchie, Phys. Rev. A **25**, 1943 (1982), and references cited therein.
[9] C. Deutsch, Laser Part. Beam **8**, 541 (1990), **10**, 355 (1992).
[10] I. Abril, M. Vičanek, A. Gras-Marti, and N. R. Arista, Nucl. Instrum. Methods B **67**, 56 (1992).
[11] M. Vičanek, I. Abril, N. R. Arista, and A. Gras-Marti, Phys. Rev. A **46**, 5745 (1992).
[12] N. R. Arista and A. Gras-Marti, J. Phys. Condens. Matter **3**, 7931 (1991).
[13] C. Deutsch and N. A. Tahir, Phys. Fluids B **4**, 3735 (1992); Nuovo Cimento A **106**, 1811 (1993).
[14] E. Nardi, Z. Zinamon, and D. Ben-Hamu, Nuovo Cimento A **106**, 1839 (1993).
[15] H. H. Mikkelsen and P. Sigmund (unpublished).
[16] Y. D'Avanzo, M. Lontano, and P. F. Bortignon, Phys. Rev. A **45**, 6126 (1992).
[17] Y. D'Avanzo, M. Lontano, and P. F. Bortignon, Phys. Rev. E **47**, 3574 (1993).
[18] F. Winterberg, Z. Phys. A **296**, 3 (1980); T. Yabe and T. Mochizuki, Jpn. J. Appl. Phys. **22**, L262 (1983).
[19] S. Eliezer, J. M. Martinez-Val, and C. Deutsch, Laser Part. Beam (to be published).
[20] N. A. Tahir, D. H. H. Hoffmann, J. A. Maruhn, and C. Deutsch, Nucl. Instrum. Methods B **88**, 127 (1994), and unpublished.
[21] A. Bret and C. Deutsch, Phys. Rev. E **47**, 1276 (1993); **48**, 2989 (1993).
[22] N. R. Arista and W. Brandt, Phys. Rev. A **23**, 1898 (1981).
[23] B. D. Fried and S. D. Conte, *The Plasma Dispersion Function* (Academic, New York, 1961).
[24] C. Deutsch, Phys. Rev. E **51**, 619 (1995).
[25] See, for instance, D. Gardés, A. Servajean, B. Kubica, C. Fleurier, D. Hong, C. Deutsch, and G. Maynard, Phys. Rev. A **46**, 5101 (1992).
[26] K. Tsuruta and S. Ichimaru, Phys. Rev. A **48**, 5101 (1992).

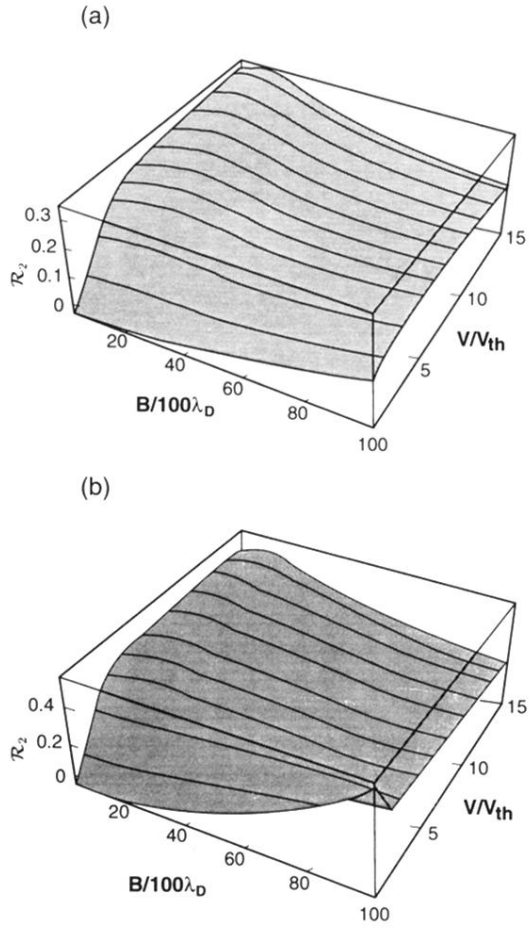

FIG. 2. (a) Ratio $\mathcal{R}_2$ [Eq. (10)] for a dicluster with $Z_1=Z_2=Z$ and $R=\lambda_D$ in terms of $B/100$ in λ_D and V in V_{th}. $T=2$ eV and $n_e=2\times10^{17}$ cm^{-3}. (b) Same as (a), but with $T=2$ eV and $n_e=10^{20}$ cm^{-3}.